

This is an Open Access document downloaded from ORCA, Cardiff University's institutional repository: <https://orca.cardiff.ac.uk/id/eprint/113014/>

This is the author's version of a work that was submitted to / accepted for publication.

Citation for final published version:

Rau, Gabriel C., Acworth, R. Ian, Halloran, Landon J. S., Timms, Wendy A. and Cuthbert, Mark O. 2018. Quantifying compressible groundwater storage by combining cross-hole seismic surveys and head response to atmospheric tides. *Journal of Geophysical Research: Earth Surface* 123 (8) , pp. 1910-1930. 10.1029/2018JF004660

Publishers page: <http://dx.doi.org/10.1029/2018JF004660>

Please note:

Changes made as a result of publishing processes such as copy-editing, formatting and page numbers may not be reflected in this version. For the definitive version of this publication, please refer to the published source. You are advised to consult the publisher's version if you wish to cite this paper.

This version is being made available in accordance with publisher policies. See <http://orca.cf.ac.uk/policies.html> for usage policies. Copyright and moral rights for publications made available in ORCA are retained by the copyright holders.



1 **Quantifying compressible groundwater storage by combining**
2 **cross-hole seismic surveys and head response to atmospheric**
3 **tides**

4 **Gabriel C. Rau^{1,2*}, R. Ian Acworth^{1,2}, Landon J. S. Halloran³,**
5 **Wendy A. Timms^{1,4}, Mark O. Cuthbert^{1,5}**

6 ¹Connected Waters Initiative Research Centre (CWI), UNSW Sydney, Australia

7 ²Water Research Laboratory (WRL), School of Civil and Environmental Engineering, UNSW Sydney, Australia

8 ³Centre d'Hydrogéologie et de Géothermie (CHYN), Université de Neuchâtel, Switzerland

9 ⁴School of Mining Engineering, UNSW Sydney, Australia

10 ⁵School of Earth and Ocean Sciences, Cardiff University, Cardiff, United Kingdom

11
12 **Key Points:**

- 13 • Cross-hole seismic surveys and tidal head analysis can be combined to improve esti-
14 mates of specific storage
- 15 • We have developed an upper bound for specific storage for unconsolidated materials
16 with low adsorbed water fractions
- 17 • Derived values of specific storage larger than this upper bound imply inappropriate
18 use of oversimplified hydrogeological conceptual models
-

19
20

*Water Research Laboratory, 110 King Street, Manly Vale NSW 2093, Australia

Corresponding author: Gabriel C. Rau (gabriel.rau@unsw.edu.au)

Abstract

Groundwater specific storage varies by orders of magnitude, is difficult to quantify, and prone to significant uncertainty. Estimating specific storage using aquifer testing is hampered by the non-uniqueness in the inversion of head data and the assumptions of the underlying conceptual model. We revisit confined poroelastic theory and reveal that the uniaxial specific storage can be calculated mainly from undrained poroelastic properties, namely uniaxial bulk modulus, loading efficiency and the *Biot-Willis* coefficient. In addition, literature estimates of the solid-grain compressibility enables quantification of subsurface poroelastic parameters using field techniques such as cross-hole seismic surveys and loading efficiency from the groundwater responses to atmospheric tides. We quantify and compare specific storage depth profiles for two field sites, one with deep aeolian sands and another with smectitic clays. Our new results require bulk density and agree well when compared to previous approaches that rely on porosity estimates. While water in clays responds to stress, detailed sediment characterization from a core illustrates that the majority of water is adsorbed onto minerals leaving only a small fraction free to drain. This, in conjunction with a thorough analysis using our new method, demonstrates that specific storage has a physical upper limit of $\lesssim 1.3 \cdot 10^{-5} m^{-1}$. Consequently, if larger values are derived using aquifer tests analysis then the conceptual model that has been used needs re-appraisal (e.g., by including vertical leakage). Our method can be used to improve confined groundwater storage estimates and refine the conceptual models used to interpret hydraulic aquifer tests.

1 Introduction

Groundwater compressible storage has always been difficult to quantify with high certainty using field techniques. Pumping-test analysis can be used to derive the aquifer properties of transmissivity and storage for a confined aquifer, but the degree of accuracy achieved for storage is often less than that achieved for transmissivity [Kruseman and de Ridder, 1990]. Theoretical approaches [Narasimhan, 1979; Narasimhan and Kanehiro, 1980] shed some light on the concept of storage and led to further discussion [Bredenhoef and Cooley, 1983; Narasimhan, 1983], with Hsieh *et al.* [1988] concluding that it was only possible to estimate S_s to within $\pm 50\%$. Wang [2000] reviewed the field of poroelasticity with applications from the geotechnical field and from hydrogeology. Specific storage is now recognized as one of the fundamental coefficients of poroelastic theory [Green and Wang, 1990], along with Young's modulus (E), the shear modulus (G), and Poisson's Ratio (μ). Its value can also vary with time due to human activity [David *et al.*, 2017]. The subject area has been overly complicated by the use of a variety of definitions and specialized terminology.

The response of a groundwater system to pumping, such as a decrease of hydraulic head or the development of land subsidence in aquitards, can only be predicted to any degree of accuracy if compressible storage properties are known at some reasonable vertical resolution [Alley *et al.*, 2002]. Although aquifer test analysis, taking account of leakage factors [Hantush, 1960, 1967a,b] and using multiple piezometers [Kruseman and de Ridder, 1990], may permit the estimation of storage properties at multiple depths, in practice these methods are not used due to the time and expense required to establish a site and the great length of time (weeks to months) required to obtain representative responses in lower hydraulic conductivity layers. Traditionally, characterization at $\lesssim 1$ m scale could be achieved through expensive sediment coring using sophisticated drilling equipment and laboratory assessment, but the validity of laboratory measurements over in-situ measurements has also been questioned [Clayton, 2011]. The accelerating depletion of global groundwater resources [Wada *et al.*, 2013; Gleeson *et al.*, 2012] necessitates development of accurate and low-cost methods to routinely establish profiles of specific storage so that the accuracy of predicted drawdowns and aquitard settlement can be assessed.

Acworth *et al.* [2016a] described a new method to quantify *in situ* barometric efficiency (BE) using the hydraulic head response to atmospheric and earth tides. We refer to this as

"tidal analysis" from here onwards. Data for three different BE values across the possible range from 0 to 1.0 [Acworth *et al.*, 2016a] and for a profile of ten different depths at a single site were described [Acworth *et al.*, 2017]. Acworth *et al.* [2017] used the BE analysis to predict specific storage using the formulation of Jacob [1940]. However, Van Der Kamp and Gale [1983] and Domenico [1983] noted (independently) that the approach of Jacob [1940] was based on a one-dimensional analysis that neglects the possibility of horizontal movement and also assumes that the compressibility of individual grains is insignificant. Van Der Kamp and Gale [1983] proposed a more extensive analysis that required consideration of the compressibility of individual components of the material (β_s) and also whether the elastic coefficients used represented drained or undrained systems. Their analysis requires further data on the elastic properties, including the bulk modulus (K), the shear modulus (G), and Poisson's Ratio (μ) of the material. They noted that estimation of specific storage would be possible if these parameters were available. Wang [2000] provides a comprehensive overview of the theory of poroelasticity.

The cross-hole seismic method is well established in the geotechnical industry [Mathews *et al.*, 1994] where it is routinely used to determine profiles of Poisson's ratio (μ), shear modulus (G), and bulk modulus (K). It is a recommended investigation technique (ASTM Method D 4428/D 4428M) when carrying out design work in unconsolidated materials for foundation or tunneling design. The methodology has changed little from early work by Davis and Taylor-Smith [1980]; Davis [1989]. Despite the success and essential simplicity of the method, application to inform groundwater resource investigation appears limited [Clayton, 2011; Crice, 2011]. The cross-hole seismic method presents an opportunity to measure the variation of elastic moduli over depth. A complete profile at any vertical interval ($\lesssim 1$ m, or less) is possible, allowing for realistic visualization of actual lithological variation of these moduli with depth. In addition, as the testing is of the ground between two boreholes, it is completely *in situ*, undrained and not subject to the inaccuracies due to sampling, sample recovery and stress changes before laboratory testing.

We present a new method to quantify profiles of specific storage in unconsolidated formations *in-situ* using a rigorous interpretation of poroelastic theory [Van Der Kamp and Gale, 1983; Green and Wang, 1990; Wang, 2000]. We combine loading efficiency derived from groundwater response to atmospheric tides in piezometers at multiple depths with elastic parameters derived from cross-hole seismic surveys. This interpretation is further strengthened by comparison with detailed laboratory data on formation water content and bulk density, derived from previously reported measurements on core material data previously reported [Acworth *et al.*, 2015]. Two sites with contrasting lithology, representing the end members of sand and clay dominated deposits, illustrate the usefulness of combining two geophysical techniques to provide reasonable bounds for compressible subsurface properties and demonstrate its implications for groundwater resource investigations.

2 Methodology

2.1 Poroelastic drained and undrained terminology in hydrogeology

Quantifying specific storage relies on the assumption that subsurface poroelasticity is linear. This has seen separate development in the areas of geomechanics, petroleum engineering and hydrogeology [Wang, 2000] that has caused a wide variety of definition and terminology. For reference, definitions of all variables used in this paper are listed in the Appendix (Table 2). In our analysis it is assumed that the subsurface system remains saturated and confined at all times.

The elastic coefficients involved in poroelastic coupling vary depending upon the time taken for a load to be applied and stress to dissipate [Domenico and Schwartz, 1997; Wang, 2000]. While two end-member conditions, undrained and drained, can be distinguished, it should be recognised that real field conditions may exist anywhere on the continuum between

122 these end members depending on the relationship between the timescale of the applied stress
 123 changes, the hydraulic properties of the formation, and the distance to hydraulic boundaries.
 124 First, for rapid loading, as occurs with the passage of a seismic wave or the response to at-
 125 mospheric tides at sub-daily frequency, there may be insufficient time for water to flow in
 126 response to the increased stress and pore pressure. Therefore, the loading occurs at con-
 127 stant mass ($d\zeta/dt = 0$ where ζ is the mass of fluid) and poroelastic coefficients represent
 128 *undrained* conditions. Second, and by contrast, if the loading occurs slowly and fluid has the
 129 opportunity to redistribute, the loading occurs at constant pore pressure ($dp/dt = 0$ where
 130 p is pore pressure) and represents *drained* conditions. In this work undrained parameters are
 131 explicitly denoted with the superscript u , drained parameters have no subscript, or (u) if a re-
 132 lationship can be used interchangeably for undrained and drained values. Note here that the
 133 term *drained* should not be confused with the interpretation that subsurface pores are drained
 134 of water, i.e. when the hydraulic head in a confined aquifer is lowered below the confining
 135 layer causing unconfined conditions, as is a common interpretation in hydrogeology. In our
 136 analysis it is assumed that the subsurface system remains saturated and confined at all times.

137 2.2 Subsurface poroelastic coefficients

138 Over the small range of pressure changes caused by tides and acoustic pulses, we assume
 139 that the matrix exhibits a perfectly elastic (i.e., *Hookean*) response. If such a material is sub-
 140 jected to a uniaxial compression or tension, a linear relationship exists between the applied
 141 stress σ and the resulting strain ϵ expressed as

$$\sigma = E^{(u)}\epsilon, \quad (1)$$

142 where E is a constant of proportionality known as *Young's Modulus*. The value of the strain
 143 ϵ is the ratio of the change in line length in its deformed state l_f to its initial state l_o

$$\epsilon = \frac{l_f - l_o}{l_o} = \frac{\Delta l}{l_o}. \quad (2)$$

144 If a *Hookean* solid is subject to uniaxial compression it will shorten in the direction of com-
 145 pression and expand in the plane at right angles to the direction of compression. If ϵ_{\parallel} repre-
 146 sents the shortening in the direction of compression and ϵ_{\perp} represents the expansion in the
 147 plane at right angles to the compression, then the ratio of these two quantities is referred to as
 148 *Poisson's Ratio*

$$\mu^{(u)} = \frac{\epsilon_{\parallel}}{\epsilon_{\perp}} \leq 0.5. \quad (3)$$

149 A solid can also be deformed by means of a shear causing shear strain (ϵ) in response to the
 150 shear stress (σ). The ratio of these quantities is the shear (or rigidity) modulus

$$G = \frac{\sigma}{\epsilon}. \quad (4)$$

151 The shear modulus G is related to the Young's modulus E and Poisson's ratio μ by

$$G = \frac{E^{(u)}}{2(1 + \mu^{(u)})}. \quad (5)$$

152 In an isotropic material subject to a change in pressure, a change in volume will occur. This
 153 is described by the *bulk modulus*:

$$K = -V \frac{dp}{dV} = \rho \frac{dp}{d\rho}, \quad (6)$$

154 where p is pressure, V is volume and ρ is material density. Further relationships for K are

$$K_{(s)}^{(u)} = G \frac{2(1 + \mu_{(s)}^{(u)})}{3(1 - 2\mu_{(s)}^{(u)})} = \frac{E_{(s)}^{(u)}}{3(1 - 2\mu_{(s)}^{(u)})}. \quad (7)$$

Note that these relationships apply for solid materials (indicated as (s)) as well as interchangeably for drained or undrained (indicated as (u)) conditions, with exception of the shear modulus G , which remains the same [Wang, 2000]. In the case of a homogeneous, isotropic, elastic materials, values for any two of the shear modulus G , Young's modulus E , bulk modulus K , or Poisson's ratio μ (or, additionally, the longitudinal modulus or Lamé's first parameter) are sufficient to define the remaining parameters for drained or undrained conditions [Wang, 2000].

2.3 Confined groundwater storage in a poroelastic formation

Wang [2000] provides a detailed analysis of poroelastic theory for both drained and undrained conditions, and *Van Der Kamp and Gale* [1983] develop expressions for the analysis of atmospheric and Earth tides, the expression of which in groundwater level time-series are normally considered as undrained phenomena. The developments build on the coupled equations for stress and pore pressure derived by *Biot* [1941] for very small deformations, typical of those that occur with the passage of seismic waves or in response to atmospheric tides. In the most general case, it is necessary to consider a fully deformable medium in which all components are compressible. Besides the bulk formation compressibility $\beta = 1/K$, which is the reciprocal of the bulk modulus $K = 1/\beta$, two more components require consideration. The water compressibility:

$$\beta_w = \frac{1}{K_w} \approx 4.58 \cdot 10^{-10} \text{ Pa}^{-1}. \quad (8)$$

The solid grain (or unjacketed) compressibility

$$\beta_s = \frac{1}{K_s} \quad (9)$$

assumes homogeneous solids and is not well defined for mixtures of different grain types [Wang, 2000].

The volume of water displaced from a sediment is always less than the change in bulk volume whenever grain compressibility is included [Domenico and Schwartz, 1997]. To take account of this change, the *Biot-Willis* coefficient is used [Biot, 1941; Wang, 2000]

$$\alpha = 1 - \frac{\beta_s}{\beta} = 1 - \frac{K}{K_s}. \quad (10)$$

Note that if $\beta_s \ll \beta$ then there is relatively little, if any, change in volume of the grains when compared to the total volume change and therefore $\alpha \rightarrow 1$.

Van Der Kamp and Gale [1983] and *Green and Wang* [1990] presented a comprehensive relationship for specific storage that assumes only uniaxial (vertical) deformation (zero horizontal stress) and includes solid grain compressibility:

$$S_s = \rho_w g \left[\left(\frac{1}{K} - \frac{1}{K_s} \right) (1 - \lambda) + \theta \left(\frac{1}{K_w} - \frac{1}{K_s} \right) \right], \quad (11)$$

where the density of water $\rho_w = 998 \text{ kg/m}^3$, the gravitational constant is $g = 9.81 \text{ m/s}^2$, θ is total porosity, and

$$\lambda = \alpha \frac{2(1-2\mu)}{3(1-\mu)} = \alpha \frac{4G}{3K_v}. \quad (12)$$

Here, K_v is the drained vertical (or constrained) bulk modulus and expressed as [Green and Wang, 1990; Wang, 2000]

$$\frac{1}{K_v^{(u)}} = \beta_v^{(u)} = \frac{1 + \mu^{(u)}}{3K^{(u)}(1 - \mu^{(u)})} = \left(K^{(u)} + \frac{4}{3}G \right)^{-1}. \quad (13)$$

188 If the solids are incompressible ($\beta_s = 1/K_s \rightarrow 0$) then Equation 11 reduces to the well-
 189 known formulation [Jacob, 1940; Cooper, 1966]

$$S_s = \rho_w g \left(\frac{1}{K_v} + \frac{\theta}{K_w} \right) = \rho_w g (\beta_v + \theta \beta_w), \quad (14)$$

190 We note that if $\mu^{(u)} = 0.5$ then it can be seen from Equation 13 that $K_v^{(u)} = K^{(u)}$. Note
 191 however, that this will only be the case for very unconsolidated silts or clays.

192 To summarize, specific storage values derived from Equations 11 and 14 represent verti-
 193 cal and isotropic stress only and are therefore smaller compared to the case where horizontal
 194 stress and strain is allowed to occur [Wang, 2000]. However, this is a reasonable and com-
 195 mon assumption which suffices to represent the conditions encountered in a hydrogeological
 196 setting. For example, Equation 14 is widely used in hydrogeology [Van Der Kamp and Gale,
 197 1983], particularly for the analysis of head measurements obtained from aquifer testing [e.g.,
 198 Kruseman and de Ridder, 1990; Verruijt, 2016].

199 2.4 Elastic moduli from the propagation of seismic waves

200 Two fundamental wave motions can transmit energy through a formation. The first is a
 201 compressional, or primary wave (*P*-wave) whose speed is a function of the undrained uniax-
 202 ial bulk modulus:

$$V_p = \sqrt{\frac{K_h^u}{\rho}} = \sqrt{\frac{K^u + \frac{4}{3}G}{\rho}}, \quad (15)$$

203 where K_h^u is the undrained bulk modulus [Wang, 2000, Page 60]. We have used the notation
 204 K_h^u to recognize that the wave front spreads out spherically from the source but is monitored
 205 in the horizontal plane. The geophone that is alligned in the horizontal direction and point-
 206 ing to the source detects the primary wave arrival after the wave has progressed horizon-
 207 tally through the formation. Hence, the appropriate bulk modulus derived from this velocity
 208 (Equation 15) is an undrained uniaxial (horizontal) bulk modulus (K_h^u).

209 Due to the short distances between the source and receiver and the assumed homogene-
 210 ity of unconsolidated deposits, we assume isotropic conditions and therefore that $K_v^u = K_h^u$.
 211 It is noted that it would be possible to investigate anisotropy in K^u by analysing the arrival
 212 times of the primary wave for the other two (one horizontal and one vertical) geophone com-
 213 ponents.

214 For sand and water mixtures, bulk density and total porosity of the formation are related
 215 through a simple volumetric mixing model [Jury *et al.*, 1991]

$$\rho = \rho_s(1 - \theta) + \rho_w \theta, \quad (16)$$

216 where ρ_s is the density of the solid phase (sand particles) generally assumed to be $2,650 \text{ kg/m}^3$,
 217 and the density of water $\rho_w \approx 998 \text{ kg/m}^3$.

218 The second wave motion is a shear wave (*S*-wave) that progresses through a material by
 219 motion normal to the direction of propagation:

$$V_s = \sqrt{\frac{G}{\rho}}. \quad (17)$$

220 Conveniently, the ratio of the compressional and shear wave velocities can be used to deter-
 221 mine the undrained Poisson's ratio μ^u directly [Davis and Taylor-Smith, 1980]

$$\mu^u = \frac{V_p^2 - 2V_s^2}{2V_p^2 - V_s^2} \leq 0.5. \quad (18)$$

222 Note that $V_s < V_p$.

223 2.5 Combining cross-hole seismic surveys and the groundwater response to atmo- 224 spheric tides

225 Specific storage has previously been calculated from barometric efficiency (BE) esti-
226 mates. *Acworth et al.* [2016a] developed an accurate method to quantify BE using the ground-
227 water response to atmospheric tides when influences at frequency of 2 cpd. The method is
228 given as

$$BE = \frac{S_2^{GW} + S_2^{ET} \cos(\Delta\phi) \frac{M_2^{GW}}{M_2^{ET}}}{S_2^{AT}}, \quad (19)$$

229 where S_2^{GW} is the amplitude of the hydraulic head, S_2^{ET} is the amplitude of the earth tide
230 and S_2^{AT} the amplitude of the atmospheric tide; $\Delta\phi$ is the phase difference between the Earth
231 tide and atmospheric drivers (both at 2 cpd frequency); M_2^{GW} is the amplitude of the hy-
232 draulic head and M_2^{ET} the amplitude of Earth tides at 1.9323 cpd frequency. The required
233 amplitudes and phases can be obtained using the *Fourier* transform of atmospheric and head
234 records which require a duration of ≥ 16 days with frequency of ≥ 12 samples per day [*Ac-*
235 *worth et al.*, 2016a].

236 We note that an estimate of specific storage for a formation comprising incompressible
237 grains can be made if the value of porosity is estimated [*Acworth et al.*, 2017]:

$$S_s = \rho_w g \beta_w \frac{\theta}{BE} \approx 4.484 \cdot 10^{-6} \frac{\theta}{BE}. \quad (20)$$

238 Estimating porosity can be problematic when dealing with fine-grained materials and, espe-
239 cially, smectitic clays where it is never clear what value of porosity exists due to the uncer-
240 tainty regarding the volume of adsorbed water (i.e., hygroscopic water bound to the surface
241 of the grains via molecular forces). This is due, in part, to the extreme values of surface area
242 per volume characteristic of clays, which render the proportion of water molecules that are
243 adsorbed rather than absorbed non-negligible.

244 In this paper, we develop a new method to quantify confined groundwater specific storage
245 depth profiles *in situ* by combining cross-hole seismic measurements of elastic coefficients
246 with the groundwater response to atmospheric tides. From *Wang* [2000] (Equations 3.84 and
247 3.81), a uniaxial specific storage equation can be derived as

$$S_s = \rho_w g \frac{\alpha}{K_v^u LE (1 - \alpha LE)} \quad (21)$$

248 where LE is the uniaxial loading efficiency (or tidal efficiency), which can be calculated
249 from BE as [*Domenico and Schwartz*, 1997; *Wang*, 2000]

$$LE = 1 - BE. \quad (22)$$

250 Equation 21 allows calculation of uniaxial specific storage mainly from undrained parame-
251 ters which are readily measured using field techniques, e.g. seismics and tidal analysis. A
252 discussion of α follows later.

253 *Wang* [2000] further shows that *Skempton's* coefficient can be calculated from undrained
254 parameters as

$$B = 3LE \frac{1 - \mu^u}{1 + \mu^u} = \frac{1 - K/K^u}{1 - K/K_s} \quad (23)$$

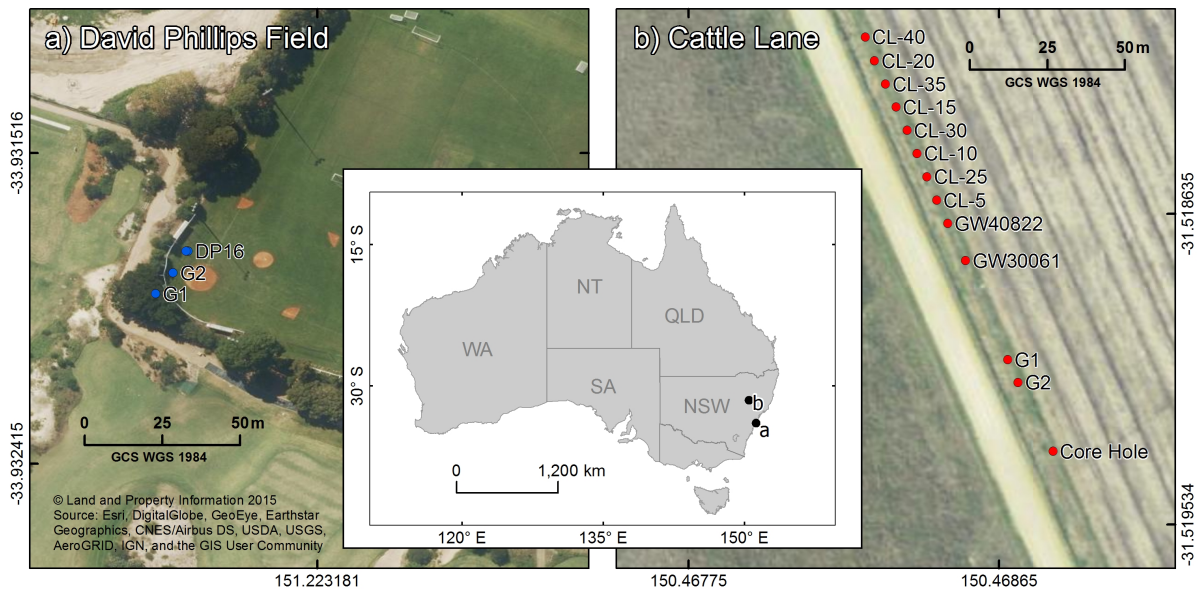
255 which can be reformulated to arrive at a relationship between undrained and drained bulk
256 modulus

$$K = \frac{K_s K^u (1 - B)}{K_s - B K^u}. \quad (24)$$

257 To quantify specific storage using our new method of combining cross-hole seismic sur-
 258 veys and tidal analysis (Equation 21), K_v^u , G and μ^u are obtained from seismic velocities
 259 (Equations 15, 17 and 18) and LE stems from tidal analysis (Equations 19 and 22). To es-
 260 timate the drained formation compressibility (24), B is calculated from seismically derived
 261 μ^u (Equation 18) and tidally derived LE (Equations 19 and 22), whereas K^u is calculated
 262 from seismically derived K_v^u and G (Equations 15 and 17). In both cases, values for K_s
 263 can be found in the literature and are discussed below.

264 2.6 Quantifying compressible groundwater storage at two field sites: Fine sands ver- 265 sus clays

266 We investigate and contrast the subsurface conditions at two field sites in Australia (Figure
 267 1) with different lithology.



268 **Figure 1.** Map showing the locations of boreholes at David Phillips Field (aeolian sand) (a) and Cattle Lane
 269 (clay) (b) in New South Wales, Australia (inset map with locations).

270 2.6.1 Sand dominated site at David Philips Field

271 David Phillips Field is located on top of the Botany Sands Aquifer in Sydney, NSW (Fig-
 272 ure 1a). During the last glacial epoch, sand has been blown from Botany Bay and now fills
 273 deep sided valleys in the Permo-Triassic Hawkesbury Sandstone [Webb and Watson, 1979;
 274 Acworth and Jankowski, 1993]. The sands provide an important water resource that, for a
 275 time, served Sydney. Webb and Watson report a very detailed pumping test at this site that
 276 determined There is an unconfined aquifer to approximately 7.5 m at the site, below which
 277 a thin layer of peat and silt acts to confine the underlying aquifer to approximately 17 m. Be-
 278 low this, a further silty sand separates a deeper confined aquifer [Webb and Watson, 1979].
 279 The depth to the water table was approximately 7 m at the time of testing. Acworth [2007]
 280 reported the results of manometer board testing from the same field that included geophys-
 281 ical logs and detail on lithology. The sands are very well sorted with a median grain size of
 282 0.3 mm and a typical porosity of $\theta \approx 0.35$ [Acworth and Jankowski, 1993].

283 Three bores were installed in the south-west corner of David Phillips Field (Figure 1a).
 284 The first bore penetrated Hawkesbury Sandstone (Permo-Triassic) at 31 m using a combi-
 285 nation of rotary auger and rotary mud drilling. The bore was completed at 36 m with
 286 80 mm PVC casing. Cement grout was placed at the base of the sands and the formation
 287 above allowed to collapse back onto the PVC casing (Borehole G1 in Figure 1a). A second
 288 bore was installed using hollow-stem augers to a depth of 28 m (Borehole G2 in Figure 1a),
 289 while a third bore was installed to 16 m depth (DP16 in Figure 1a). Both these bores were
 290 completed using 50 mm PVC with a 1 m screen set at the base.

291 Water level data for the Botany Site at David Phillips Field were measured in piezometer
 292 DP16. A Diver data logger was used with a sampling interval of 1 hour. The atmospheric
 293 pressure was compensated using the record from Sydney Airport (≈ 4 km from the field site).
 294 There is only a single value of barometric efficiency ($BE = 0.151$) available for David
 295 Phillips Field from Piezo-16 (Figure 1a).

296 **2.6.2 Clay dominated site on the Liverpool Plains**

297 The second field site, Cattle Lane, is located on the Liverpool Plains, NSW (Figure 1b).
 298 Deposition of clay derived from the nearby Liverpool Ranges has occurred onto the Liver-
 299 pool Plains (south to the north). The saturated zone at this site is typically within a meter or
 300 two of the ground surface. Clay deposition has been dominant during drier periods, with silt
 301 and clay deposited during colder periods and gravels and sands during periods of higher rain-
 302 fall. This sequence has been proven by coring ('Core Hole' on Figure 1a) to 31.5 m depth
 303 and the lithology is given by *Acworth et al.* [2015]. Note that the subsurface is very homo-
 304 geneous in the horizontal direction (150 m between CL40 and the core hole, Figure 1) as
 305 determined by surface-based geophysics across the site [*Acworth et al.*, 2015].

306 To conduct the cross-hole seismic survey [*Crice*, 2011] at Cattle Lane, two boreholes
 307 were drilled to 40 m depth adjacent to the cored hole (G1 and G2 shown in Figure 1). The
 308 boreholes were lined with thin-walled PVC casing that was grouted in place using a weak ce-
 309 ment/mud slurry forced out of the base of the casing and allowed to overflow back to the sur-
 310 face outside the casing, ensuring that no air gaps were present. Good continuity was achieved
 311 between the formation and the casing with no air gaps to ensure unrestricted passage of seis-
 312 mic waves.

313 Bulk densities were measured on the clay samples recovered from the core nose of the
 314 triple-tube core barrel [*Acworth et al.*, 2015] immediately after sample collection. Densi-
 315 ties corresponding to the depths of the cross-hole measurements were calculated by inter-
 316 polation of measurements at known depths. Samples were also dried and weighed to obtain
 317 total moisture and bulk density data (Table 1). Essential data for the core measurements at
 318 the site are presented in Table 1.

323 There are a total of nine piezometers screened at 5 m intervals between 5 and 55 m
 324 depth exist at Cattle Lane. Water levels were measured in these piezometers using vented
 325 pressure transducers (LevelTroll, InSitu Inc, USA). We note that the subsurface processes
 326 at this site are relatively well understood and have been reported in a number of previous
 327 papers. For example, in prior studies, the lithology was sampled by obtaining minimally dis-
 328 turbed 100 mm core followed by extensive laboratory testing and analysis [*Acworth et al.*,
 329 2015] and the barometric efficiency and degree of confinement over depth established [*Ac-*
 330 *worth et al.*, 2016a, 2017]. We extensively make use of this existing dataset in order to add
 331 context to the cross-hole seismic survey and further improve our understanding of the uncon-
 332 solidated subsurface.

333 **2.7 Cross-hole seismic survey procedure**

334 At both sites, a seismic source (Ballard borehole shear wave source) was lowered into the
 335 borehole and clamped to the casing using an inflatable bladder expanded using air pressure.

Core Sample Depth z (m BGS)	Water Content θ (%)	Natural Density ρ (kg/m^3)	Free-water Porosity θ_{free} (%)	Piezo Depth z (m)	BE (-)
2.68	64.71	1659	0.015	5	0.010
4.35	31.25	1907	0.010	10	0.007
5.85	43.48	1926	0.007	15	0.032
7.35	46.43	1864	0.007	20	0.039
10.35	52.94	1721	0.007	25	0.042
11.85	47.37	1707	0.005	30	0.042
13.35	36.36	1997	0.020	35	0.059
14.85	58.57	1763	0.018	40	0.121
16.40	48.44	1664	0.018	55	0.138
17.35	47.37	1748	0.020		
19.35	52.38	1721	0.023		
20.85	55.56	1821	0.023		
22.35	45.45	1807	0.020		
23.85	52.63	1815	0.020		
26.85	36.17	1924	0.020		
28.35	34.29	1940	0.020		
29.85	44.99	1756	0.022		
31.35	25.00	2075	0.023		

319 **Table 1.** Depth profile of moisture content and density for core samples [Acworth *et al.*, 2015] and *BE*
320 values from piezometers [Acworth *et al.*, 2017] at the Cattle Lane site. Note: Estimates of free-water porosity
321 (θ_e) are based upon the analysis of density developed in Section 3.1.2. BGS = "below ground surface." BE =
322 "barometric efficiency"

336 Upward and downward polarized shear waves were generated by either dropping a weight
337 onto the clamped frame or pulling the weight upwards so that it struck the clamped frame.
338 P-waves were generated by both upward and downward blows on the clamped frame. Seis-
339 mograms were recorded using a submersible three-component geophone (Geostuff wall-
340 lock geophone). The geophone had two horizontal and one vertical element and was locked
341 in place using a mechanical arm (steel spring) that was activated from the surface. The hor-
342 izontal components were configured so that one component was normal to the source bore
343 and the second at right angles using an on-board magnetometer element to sense direction.

344 Seismograms were recorded by a multi-channel seismograph using image stacking to im-
345 prove the signal-to-noise ratio. In general, six upward and six downward blows provided a
346 clear indication of the shear wave arrival. Data was collected either at 0.5 m or 1.0 m inter-
347 vals, but the station interval was arbitrary. Data collection required between 2 and 3 hours
348 work. The distance between the shot and receiver bores at different depths was established by
349 running borehole verticality logs (Geovista verticality sonde) in each bore. The verticality-
350 distance relationships were combined to calculate the distance between the source and re-
351 ceiver at each required depth. Wave arrival times were estimated using the vertical compo-
352 nent for the shear waves and the beginning of the phase difference between the upward and
353 downward blows. Similarly, the compressional wave arrivals were estimated using the hor-
354 izontally orientated geophones. Wave velocities were established using the horizontal dis-
355 tance between the sensors established from the verticality survey .

3 Results and Discussion

3.1 Combining cross-hole seismic surveys and tidal analysis reveals subsurface properties

Example primary and shear wave measurements are shown in Figure 2 to illustrate the data collected from the three-component geophones. The *P*-wave arrivals are noticeably in phase, whereas the *S*-wave arrivals are 180° apart. As the vertical component presents the clearest arrival time, it is used in the investigation of shear-wave anisotropy.

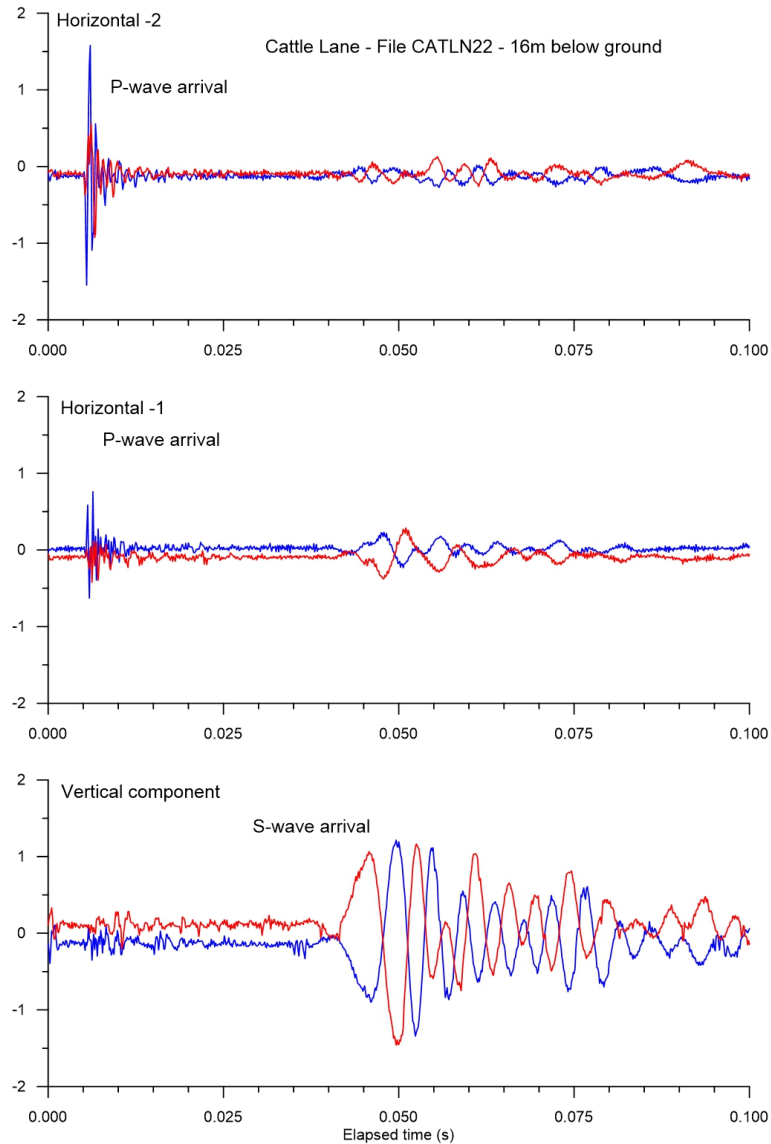
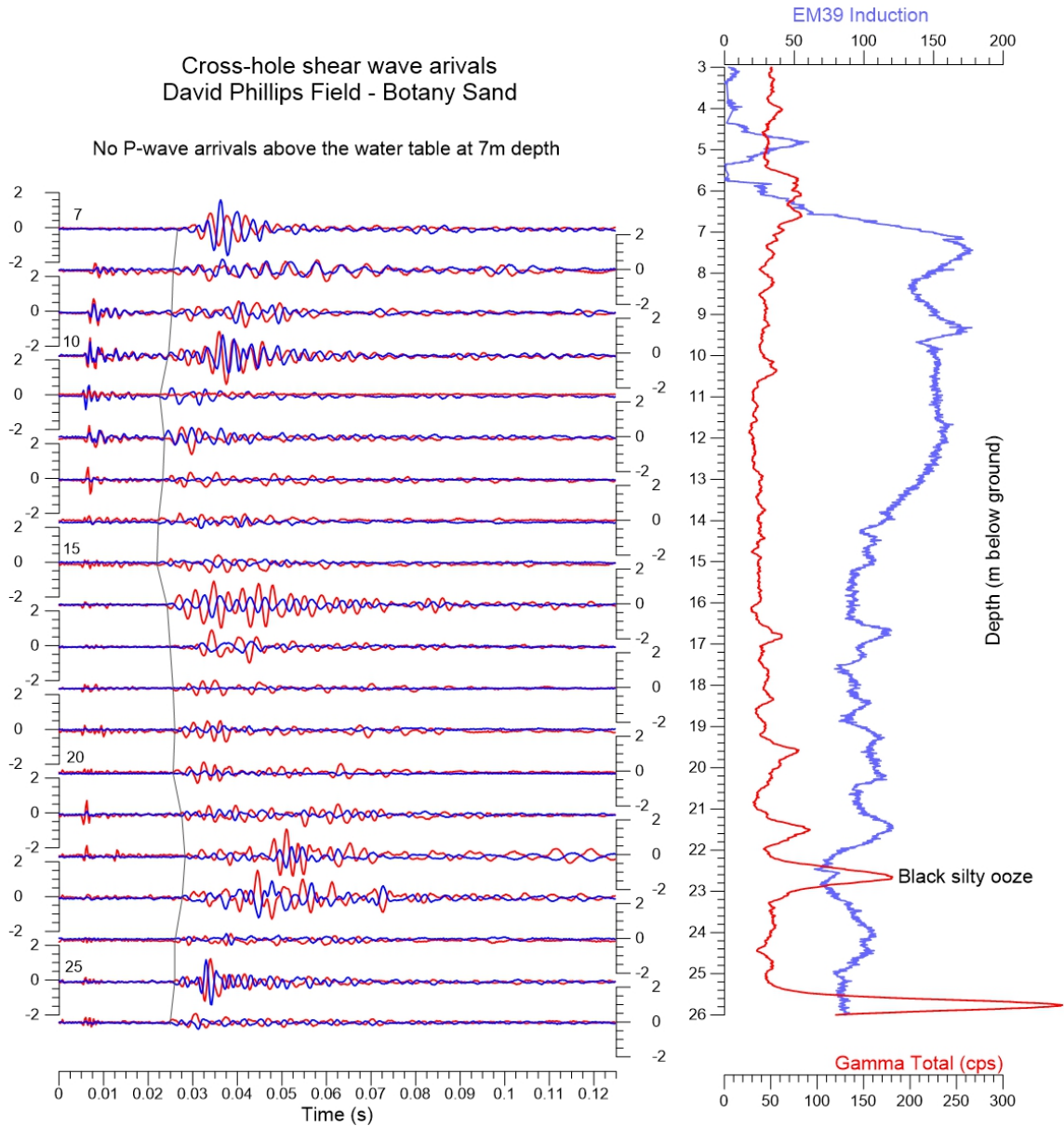


Figure 2. Example output from the three-component geophone showing the arrivals from upward (red) and downward (blue) polarities measured at 16 m BGS at Cattle Lane (Figure 1b).

We calculate the drained and undrained poroelastic parameters from undrained measurements using values for grain compressibility provided in the literature. Further, two different specific storage depth profiles are calculated and compared: (1) Equation 20: This approach

368 assumes a porosity as well as incompressible grains ($K_s = 0$); (2) Equation 21: In this new
 369 method, the required parameters are obtained by combining cross-hole seismic surveys and
 370 tidal analysis. Here, it is noteworthy that the bulk density ρ is required instead of porosity.
 371 Further, the influence of compressible grains can be explored by taking K_s values from the
 372 literature. This mathematically constrains the poroelastic parameter space so that K values
 373 can be obtained from Equation 24.

374 **3.1.1 Sand dominated site: David Phillips Field**



375 **Figure 3.** Profile of the vertical component cross-hole survey results from bore G2 at David Phillips Field
 376 (Figure 1a) vertically co-located with an EM39 induction and gamma depth survey.

The seismic waveforms (Figure 3) measured during the cross-hole survey at David Phillips Field are shown along with the gamma-ray activity and bulk electrical conductivity (EC) logs to provide a lithological comparison. The water level in the sands at the time of measurement was ~ 7 m below ground surface. Both P - and S -wave arrivals were detected above this depth. Elevated bulk EC levels between 7 m and 15 m represent contaminated groundwater moving laterally from an old waste fill and the elevated gamma-ray activity at 23 m is considered to be an old inter-dune wetland that may have trapped dust [Acworth and Jorstad, 2006].

The shear wave results for the David Phillips Field (Figure 3) indicate that there is significant variation in signal amplitude with depth, although the source signal was produced manually, i.e. by pulling up or letting the shear source weight drop down. This suggests that the shear wave amplitude could be used to indicate lithological variability. The sedimentary sequence at this site was examined during drilling to comprise uniform sands to 22 m depth with a black silty ooze at 23 m before a return to uniform sands. Samples were not kept as the sequence appeared so uniform.

Shear-wave amplitudes suggest that considerably greater variability is present that may indicate differences in consolidation or proto-soil development due to a break in sand accumulation. The sequence is undated although tree remains from approximately 30 m at a site in the sands 800 m to the southwest give an uncorrected radio-carbon date of $\sim 30,000$ BP. Variability in sediment accumulation rate and type would have occurred through the last glacial maximum at this site.

The results derived from the cross-hole survey at David Phillips Field are shown in Figure 4a (and presented in Table S1). In the absence of depth-specific information, a density of $\rho = 2,072 \text{ kg/m}^3$ was determined using Equation 16 with a total moisture content $\theta = 0.35$ [Acworth and Jankowski, 1993]. As a first approximation, porosity, density and loading efficiency were not considered to vary with depth. Fine-grained sands with thin beds of silt/clay at the site were reported by Webb and Watson [1979]. The barometric efficiency measured in the piezometer installed at 16 m ($BE = 0.151$) was used to calculate the loading efficiency ($LE = 0.849$, Equation 22).

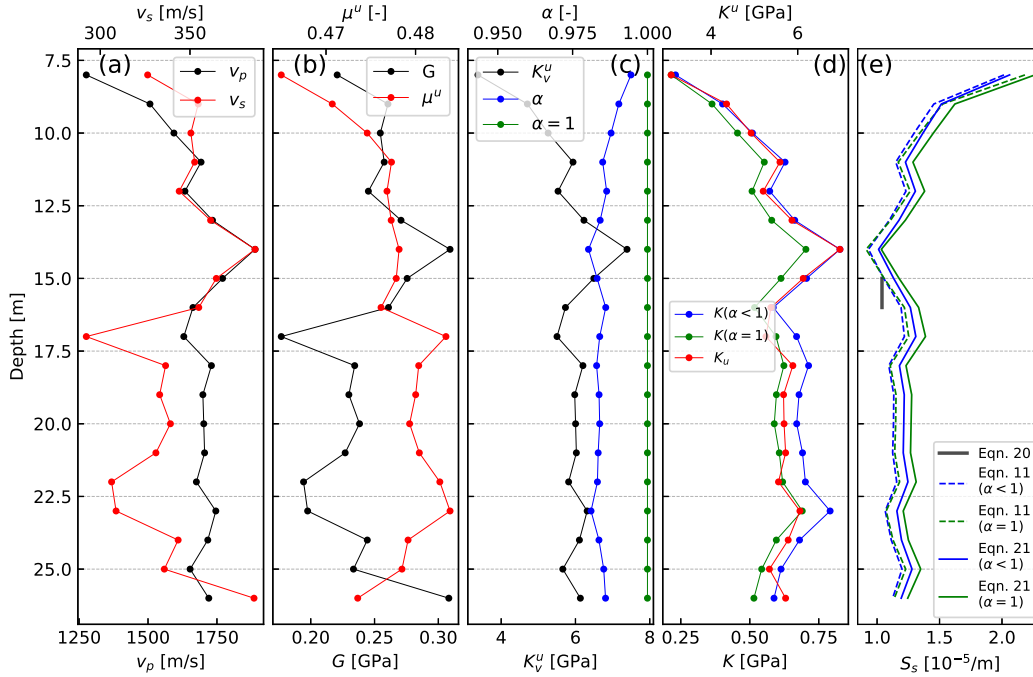
Richardson *et al.* [2002] report a solid grain modulus for Ottawa Sand in the range of $30 \leq K_s \leq 50 \text{ GPa}$ using 95% confidence limits, which they consider to be consistent with values for polycrystalline quartz found in the literature ($36 \leq K_s \leq 40 \text{ GPa}$) and also for glass beads. The Ottawa Sands had a fractional porosity of 0.373, a mean P -wave velocity of $1,775 \text{ m/s}$, a bulk density of $2,080 \text{ kg/m}^3$ and a grain density of $2,670 \text{ kg/m}^3$. As the physical properties of the Ottawa Sand sample closely match those from David Phillips Field, we have selected the mid point of the solid grain modulus range ($K_s = 42 \text{ GPa}$), which represents a $\beta_s \approx 2.632 \cdot 10^{-11} \text{ Pa}^{-1}$, for our poroelastic analysis.

The results of the poroelastic calculations are summarized in Figure 4. Figures 4b-d show the calculated depth profiles for the poroelastic coefficients. Figure 4e compares the three specific storage estimates calculated using:

- Equation 20 (for the single value of LE at 16 m depth). This is the conventional analysis that is based upon Jacob [1940] and is implemented in Acworth *et al.* [2017];
- Equation 11 with values calculated for $K_s = 42 \text{ GPa}$ ($\alpha <$) as well as $K_s \rightarrow \infty$ ($\alpha = 1$). This is a fully developed poroelastic solution where knowledge of parameters are required, i.e. estimates for porosity, drained bulk modulus K , solid grain modulus K_s , and shear modulus G or Poisson ratio μ ;
- Equation 21 with values calculated for $K_s = 42 \text{ GPa}$ ($\alpha <$) as well as $K_s \rightarrow \infty$ ($\alpha = 1$). This is the new poroelastic approach presented in this paper which requires density estimates.

We note the agreement between the three specific storage calculations (Figures 4e). The values of specific storage decrease from $S_s \approx 2 \cdot 10^{-5} \text{ m}^{-1}$ to $S_s \approx 1.2 \cdot 10^{-5} \text{ m}^{-1}$ over depth. We

427 note also that bulk density and porosity are related (Equation 16), an observation that we will
 428 return to below.



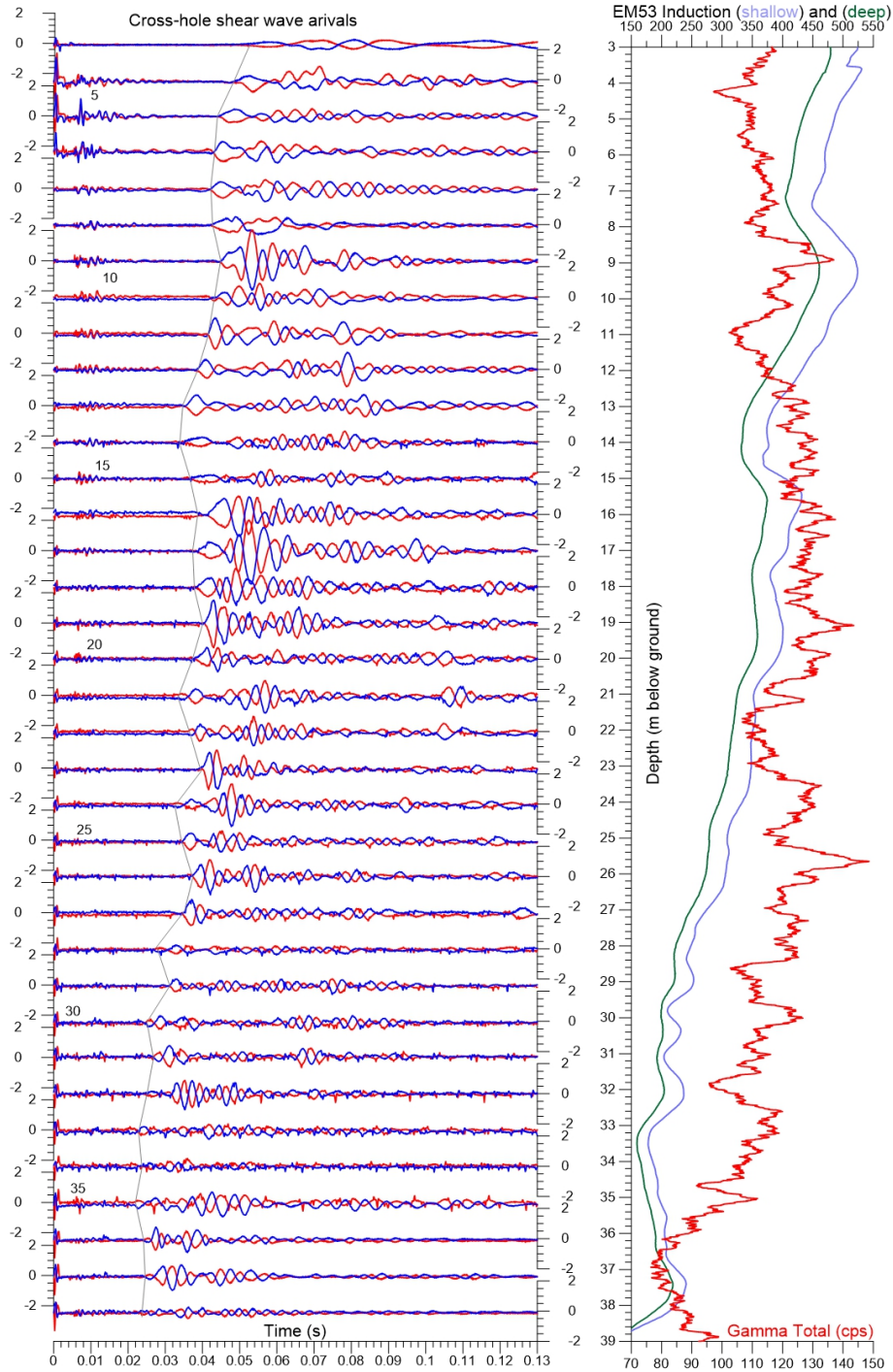
429 **Figure 4.** Results for the David Phillips Field Site (a) Primary and shear wave velocity data; (b) Undrained
 430 Poisson's Ratio and Shear modulus (c) *Biot-Willis* coefficient (α) and undrained (vertical) bulk modulus (K_v^u)
 431 (d) Drained (K) and undrained (K^u) bulk moduli (e) Specific storage estimates using parameter ranges as
 432 described in the text.

3.1.2 Clay dominated site: Cattle Lane

433
 436 The seismic waveforms recorded during the cross-hole survey by the vertically orientated
 437 geophone at Cattle Lane are shown in Figure 5. The depth of each seismogram is arranged so
 438 that the zero amplitude is adjacent to the depth below ground level used for the geophysical
 439 logs. The associated seismic velocity analysis is presented in Table S2 of the Supplementary
 440 Information.

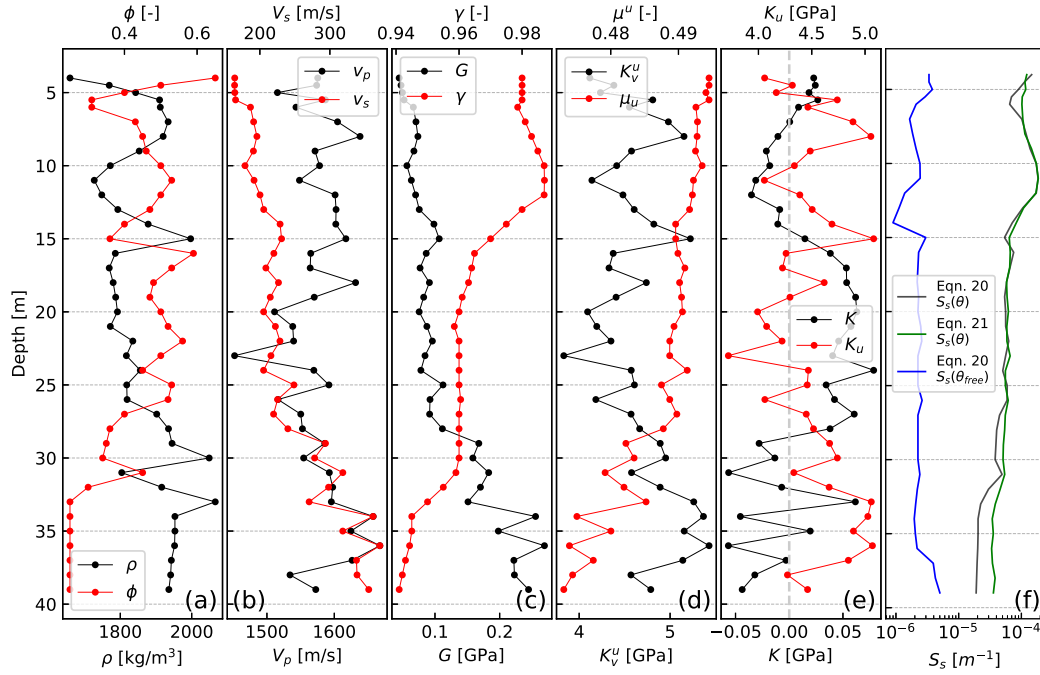
441 A detailed lithological characterization for this site has previously been published [Ac-
 442 worth *et al.*, 2015, 2016a] and provides physical data and observations that we draw upon for
 443 the poroelastic analysis in this work. S-wave variability was significantly higher at this site
 444 than at David Phillips Field. It is therefore assumed that the observed variability is a function
 445 of lithology and not a measurement artifact. The shear-wave data was collected to 38 m,
 446 a depth that correlates to an age of approximately 150 ka [Acworth *et al.*, 2015] and covers the
 447 start of the penultimate glacial, the interglacial and the last glacial stages of the Ice Age.

448 It is not the intention to fully interpret the correlations between the shear-wave arrivals
 449 and waveforms but to note that there appear to be relationships between shear waveforms
 450 and the past climate variations that cause the different lithologies observed. For example, the
 451 clear change in shear waveform at 14 and 15 m depth (much reduced amplitude and lower
 452 frequency) shown in Figure 5 correlates with the depth at which Acworth *et al.* [2015] ob-



434 **Figure 5.** Profile of the vertical component cross-hole survey results at Cattle Lane arranged alongside with
 435 the gamma-ray activity and electromagnetic borehole logs

453 served a sandy layer in the bore during construction. Core recovery over this interval was
 454 very poor and good core only recommenced at 16.5 m. The age of sediments at this depth
 455 is approximately 55 to 60 ka *Acworth et al. [2015]* and correlates with *lake full* conditions



461 **Figure 6.** Depth profiles of the poroelastic parameters at the Cattle Lane Field Site (a) Porosity and density
 462 (b) Seismic velocities (c) Loading efficiency and shear modulus (d) Poisson's ration (undrained) and bulk
 463 modulus (vertically constrained and undrained) (e) Undrained vertical bulk modulus and undrained bulk mod-
 464 ulus (f) Specific storage, quantified using Equation 20 assuming a measured bulk moisture content as total
 465 porosity θ (black line) and using Equation 21 with measured formation densities (green line). For smectite
 466 clays we assumed that $\alpha = 1$. For comparison, S_s calculated from the free water fraction $S_s(\theta_{free})$ is shown.

466 across eastern Australia [Bowler, 1990] as well as a period of increased dust concentration
 467 in Antarctic ice-cores [Petit et al., 1999]. Shear waveforms remain stronger between 16 and
 468 21 m depth (65 to 80 ka) during a time of reduced dust and higher temperatures. It is evi-
 469 dent that the seismic shear waves could be further analyzed for an improved correlation with
 460 lithology.

467 A solid-grain modulus for the smectite dominated clay at the Cattle Lane Site is also re-
 468 quired to mathematically constrain the poroelastic relationships. However, no data are avail-
 469 able for Cattle Lane and we have not found values for smectite dominated clay in the liter-
 470 ature. This is not surprising as the parameter is intrinsically difficult to measure given the
 471 fact that a high proportion of the water associated with the clay is adsorbed. Separating the
 472 clay from the water changes the material matrix. Prasad et al. [2001] directly measured
 473 Young's modulus and Poisson's Ratio of clay minerals and found values of $E_s = 5.9 \text{ GPa}$
 474 and $\mu_s = 0.3$. These values can be converted to a clay solid gain modulus $K_s \approx 4.9 \text{ GPa}$
 475 (Equation 7). However, this result leads to negative and therefore physically unrealistic val-
 476 ues of K when Equation 24 is used. We hypothesize that the assumed linearity inherent to
 477 poroelastic theory breaks down for clays, a fact that has been noted before [Bathija, 2000].
 478 We therefore make the reasonable assumption that $K_s \gg K$ and that the Biot-Willis coeffi-
 479 cient $\alpha = 1$ for smectite clays.

480 The cross-hole survey results for Cattle Lane are shown in Figure 6b. Note that this is
 481 accompanied by existing depth specific total moisture (porosity) and bulk density provided

482 by laboratory measurements in Figure 6a [Acworth *et al.*, 2015]. Again, the depth profiles
 483 of specific storage were calculated using Equations 20 and 21 with measured and estimated
 484 (interpolated) values of θ and ρ .

485 Our new method for calculating specific storage (Equation 21) relies on an estimate of the
 486 formation bulk density, whereas Equation 20 necessitates knowledge of the total porosity.
 487 The excellent match between both results confirms the accuracy of our laboratory based mea-
 488 surements from the core reported in Acworth *et al.* [2015]. These density and moisture con-
 489 tent profiles were interpolated between field laboratory measurements for the clays at Cattle
 490 Lane to estimate values at the depths of the seismic measurements. An extended density for-
 491 mulation was required for the clay sites as it was not possible to use Equation 16 to replicate
 492 the higher bulk densities measured in the core samples. In recognition of the fact that much
 493 of the total moisture (θ) is adsorbed into the clay matrix, Equation 16 was extended to in-
 494 clude a fraction of the total moisture as adsorbed moisture with a higher density [Martin,
 495 1960; Galperin *et al.*, 1993] as follows:

$$\rho = \rho_s(1 - \theta) + \rho_{ads}\theta_{ads} + \rho_w\theta_{free}, \quad (25)$$

496 where θ is the field measured moisture content, θ_{ads} is the adsorbed moisture fraction, and
 497 $\theta_{free} = \theta - \theta_{ads}$ is the free-water fraction; ρ_s is the solid density (between 2,000 and
 498 2,700 kg/m^3 based upon published values), ρ_{ads} is the adsorbed water density (between
 499 1,000 and 1,400 kg/m^3) [Martin, 1960; Galperin *et al.*, 1993]. We note that the value of
 500 θ_{free} represents the water that can freely drain from the formation and is considered similar
 501 to the specific yield S_y value that would occur when the system becomes unconfined. With
 502 this approach, predicted values of density could be found that matched the observed natural
 503 densities by using an adsorbed water density of 1,400 kg/m^3 . The intervening depths were
 504 then estimated using the determined range of values.

505 Water adsorbed onto clay minerals is recognized as having physical properties more akin
 506 to the solid than the fluid with considerable viscosity, elasticity and shear strength [Galperin
 507 *et al.*, 1993]. Considerable uncertainty concerns the physical properties of adsorbed water in
 508 the literature and its implications for groundwater resources or geotechnical understanding
 509 are unknown. Our results demonstrate that the response of clays and adsorbed water to stress
 510 can be fully explained by poroelastic theory using the total moisture content. This is to be
 511 expected because seismic waves and the loading efficiency stresses must act upon the total
 512 mass present. However, predicted specific storage values calculated using poroelastic theory
 513 assuming porosity is equal to the total water content will likely lead to large overestimates.
 514 This is because, as Equation 25 indicates, only a very limited proportion of the water present
 515 in the clays - that which is not adsorbed to the clay mineral structure - will be free to flow in
 516 and out of the pores and therefore contribute to the specific storage value. We calculate this
 517 quantity from the theoretical analysis of density (Equation 25). We note that the very low
 518 values of free-water porosity are corroborated by the field observation that the cores were
 519 almost dry to touch with little free water noted [Acworth *et al.*, 2015].

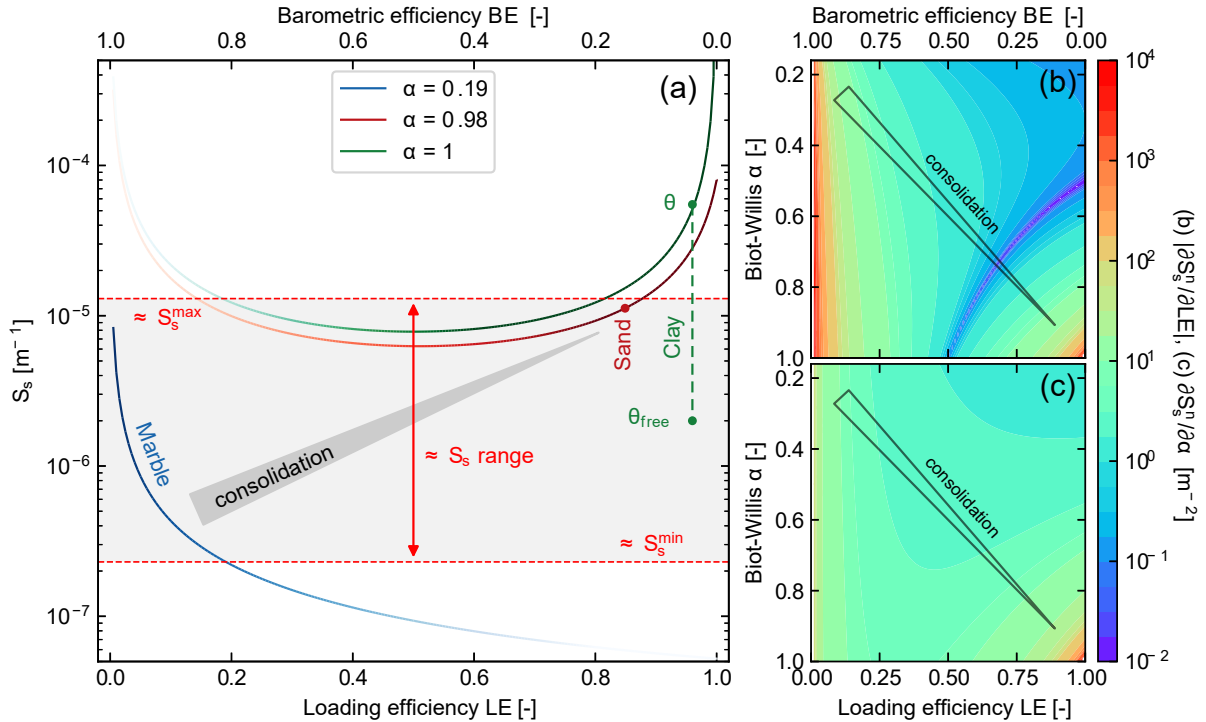
520 Our estimates of the free water in the clays (θ_{free}) are shown in Table 1 and have been
 521 used to re-evaluate the possible range of specific storage values via Equation 11. The results
 522 are shown by the blue line in Figure 6f and demonstrate that realistic values of specific stor-
 523 age for smectite clays are approximately $2 \cdot 10^{-6} m^{-1}$ consistent with previous work by Ac-
 524 worth *et al.* [2017, Table 1].

525 3.2 Analysis of the poroelastic parameter space for specific storage and its limits

526 We analyze the influence of the parameters involved in predicting specific storage us-
 527 ing Equation 21 while aiming to better understand the interplay of the various components
 528 across the spectrum of consolidation found in real environments. Equation 21 relies only on
 529 three parameters, the undrained vertical bulk modulus K_v^u , the loading efficiency LE and the

530 *Biot-Willis* coefficient α . We also investigate the sensitivity to LE and α when Equation 21 is
 531 made independent of physical constants, i.e. $S_s^m = S_s \cdot K_u^v \cdot g \cdot \rho_w$.

532 We used the published poroelastic parameters for marble ($\alpha = 0.19$ [-]; $K = 40$ GPa; K_u
 533 = 44 GPa and $G = 24$ GPa) reported in [Wang, 2000, Table C.1] which represents the most
 534 consolidated conditions measured in the literature. The undrained vertical bulk modulus K_u^v
 535 was derived using Equation 13. To represent unconsolidated conditions, we used the results
 536 presented earlier (Section 3.1). In our analysis, we assume that the loading efficiency can be
 537 calculated with good accuracy using the objective method of the groundwater response to
 538 atmospheric tides developed by Acworth *et al.* [2016a] and we allow values to vary between
 539 $0 \leq LE \leq 1$.



540 **Figure 7.** (a) Theoretical values of specific storage S_s as calculated using Equation 21 with literature values
 541 representative for the most consolidated system as well as our results representative for unconsolidated cases;
 542 (b) Sensitivity of specific storage to the loading efficiency LE , and (c) to the *Biot-Willis* coefficient α .

543 Figure 7a shows theoretical values of specific storage calculated using Equation 21 and
 544 the aforementioned parameter combinations, whereas Figures 7b and 7c illustrate the sensi-
 545 tivity of specific storage to changes in loading efficiency and the *Biot-Willis* coefficient,
 546 respectively. Note that only parts of this parameter space are reflective of real-world condi-
 547 tions, as is discussed in the following.

548 It is interesting that S_s is most sensitive to LE (Figure 7b) when this parameter assumes
 549 very high or very low values. For $\gamma \rightarrow 0$ the specific storage values obtained from Equa-
 550 tion 21 diverge and are infinitely sensitive to loading efficiencies that are either very small
 551 ($LE \rightarrow 0$) or large ($LE \rightarrow 1$). Because diverging values of S_s are physically impossible, it
 552 can be deduced that a lower bound for loading efficiency must exist such that $LE > 0 \gamma > 0$
 553 ($BE < 1$), and for values of $\alpha \rightarrow 1$ also $LE < 1 \gamma > 0$ ($BE > 0$). The sensitivity of spe-

554 cific storage to α appears to change for high values of loading efficiency (Figure 7c), such as
 555 is characteristic of water-saturated clays (Figure 7a). As such, elastic clay represents the most
 556 unconsolidated end-member with $\alpha = 1$.

557 While measurements of K_v^u exist in the literature for different materials [*Palciauskas and*
 558 *Domenico, 1989; Domenico and Schwartz, 1997; Wang, 2000*], little is known about how LE
 559 and α relate to real-world conditions. The *Biot-Willis* coefficient α describes the inverse of
 560 the ratio between bulk compressibility and grain compressibility [*Wang, 2000*]. Here, bulk
 561 compressibility values are correlated with the ability of the formation to reduce in volume
 562 when stressed, and the micro-scale mechanism is attributed to a rearrangement of individual
 563 grains [*Wang, 2000*]. It is interesting to note that under consolidated conditions, i.e. when
 564 the grains are locked together by chemical precipitate, the possibility of this rearrangement
 565 is much smaller than when compared to unconsolidated conditions, for which potential grain
 566 movement depends on the degree of packing. This is reflected in literature values of α , e.g.
 567 for marble the ratio of solid grain compressibility is high in relation to that of the formation
 568 ($\alpha = 0.19$) whereas for clay this is very small ($\alpha = 1$).

569 The loading efficiency describes the sharing of stress induced by the weight acting on a
 570 confined groundwater system. Barometric efficiency BE and loading efficiency LE describe
 571 the relative share of stress supported by the matrix and the groundwater [*Domenico and*
 572 *Schwartz, 1997; Wang, 2000*]. To date, relationships between its value and field conditions
 573 have not been well-described in the literature. It is interesting to note that in consolidated
 574 systems (e.g., marble or limestone) the stress can be absorbed mainly by the solid matrix and
 575 therefore $LE \rightarrow 0$ ($BE \rightarrow 1$). Such formations are thought to act as a barometer where the
 576 pore pressure is negatively correlated with the atmospheric pressure [*Meinzer, 1928; Jacob,*
 577 *1940; Domenico and Schwartz, 1997*]. Contrarily, in unconsolidated systems where the stress
 578 is shared between water and matrix, the loading efficiency $LE \rightarrow 1$. Interestingly, *Acworth*
 579 *et al.* [2016a] found that $LE \approx 0.02$ ($BE \approx 0.98$) in a clayey-sand formation that existed be-
 580 neath over-consolidated clays of Tertiary age at Fowlers Gap in western NSW [*Acworth et al.,*
 581 *2016b*]. Again, this points to the fact that both γ and α can depend on how well grains are
 582 packed. An optimum packing will result in less individual grain movement and vice versa.
 583 It is therefore very difficult to determine a definitive relationship between all parameters in-
 584 volved. However, there appears to be an interrelated correlation for consolidation, here de-
 585 fined as optimum packing or grains locked in place by chemical precipitate, where $\alpha \rightarrow 0.2$
 586 and $LE \rightarrow 0$ reflect more consolidated environments (see annotation in Figure 7). Further
 587 evaluation of BE and α for different environments will lead to improved understanding of
 588 these relationships.

589 We further apply these considerations to finding realistic bounds for specific storage.
 590 From Figure 7a, a hypothetical minimum specific storage can be deduced for the poroe-
 591 lastic parameters that characterize marble by following the blue line. However, the required
 592 loading efficiency of $LE \rightarrow 1$ is unrealistic as LE must remain towards the lower end. While
 593 a realistic bound is difficult to determine, we assume that for marble or limestone $LE \lesssim 0.2$.
 594 This results in a lower bound of $S_s^{min} \approx 2.3 \cdot 10^{-7} m^{-1}$ but which must be prone to consider-
 595 able uncertainty.

596 On the other end, clays are generally thought of as having the highest values of specific
 597 storage due to their high compressibility [e.g., *Domenico and Schwartz, 1997; Fetter, 2001*].
 598 Our results demonstrate that the total moisture content responds to stress and that poroelastic
 599 theory is able to quantify parameters for unconsolidated conditions. While this allows hypo-
 600 theoretical estimates of S_s^{max} , our results further demonstrate that such values may not be mean-
 601 ingful to predict the quantity of water that is freely expelled from the clay, i.e. as is the case
 602 during groundwater pumping. It is well known that a large proportion of the total moisture
 603 content associated with a swelling clay is adsorbed water that is not readily released by sim-
 604 ple drainage [*Jury et al., 1991; Galperin et al., 1993*]. The complicated nature of the interac-
 605 tion between water and clay minerals may also thwart the assumption of linearity inherent to

606 poroelastic theory [Bathija, 2000]. It is therefore questionable whether poroelastic theory can
 607 determine an absolute upper bound S_s^{max} that is meaningful for water resources.

608 For our smectite clays, we estimate a maximum $S_s^{max}(\theta_{free}) \approx 1 \cdot 10^{-6} m^{-1}$ from values
 609 that are quantified in Figure 6, and a previous description by Acworth *et al.* [2017]. However,
 610 it appears that fine sands can have higher S_s values compared to clays (compare Figures 6
 611 and 4). While it is difficult to estimate an upper limit for extractable water, this must be based
 612 on the free water fraction and we estimate this value to be maximal at $S_s^{max}(\theta_{free}) \approx 1.3 \cdot$
 613 10^{-5} (Figure 7a) for silts or kaolinitic dominated clays where the adsorbed water fraction is
 614 lower than in smectite dominated clays [Jury *et al.*, 1991].

615 Notably, both cross-hole seismic and tidal analysis yield coefficients representative of
 616 undrained conditions. The specific storage Equations 11 and 21 contain the drained bulk
 617 K and solid grain moduli K_s . Because both parameters are unknown, the poroelastic sys-
 618 tem remains mathematically unrestrained, i.e. not all parameters can be quantified by com-
 619 bining cross-hole seismics and tidal analysis. However, the unknown moduli occur as the
 620 *Biot-Willis* coefficient α (Equation 10) in Equations 21 and 24. As discussed here, values
 621 for unconsolidated bulk moduli are generally much lower compared to consolidated forma-
 622 tions [Domenico and Schwartz, 1997; Wang, 2000]. This means that $K \ll K_s$ and therefore
 623 $K/K_s \rightarrow 0$ hence $\alpha = 1$, which leads to the following simplification of Equations 21 and 24
 624 [Wang, 2000]

$$S_s = \rho_w g \frac{1}{K_v^u LE(1 - LE)} \quad (26)$$

625 and

$$K = K^u(1 - B) = \left(K_v^u - \frac{4}{3}G \right) \left(1 - 3LE \frac{1 - \mu^u}{1 + \mu^u} \right). \quad (27)$$

626 Equations 26 and 27 mathematically constrain the parameter space and can therefore be used
 627 to approximate the poroelastic properties of unconsolidated formations using cross-hole seis-
 628 mic surveys and the groundwater response to atmospheric tides.

629 We note here that our analysis also produces a value of the drained bulk modulus (K)
 630 from Equation 24 or Equation 27 although, for the sake of brevity, the value of these esti-
 631 mates for geotechnical investigations will be described in a subsequent paper.

632 3.3 Implications for groundwater resource analysis and modeling

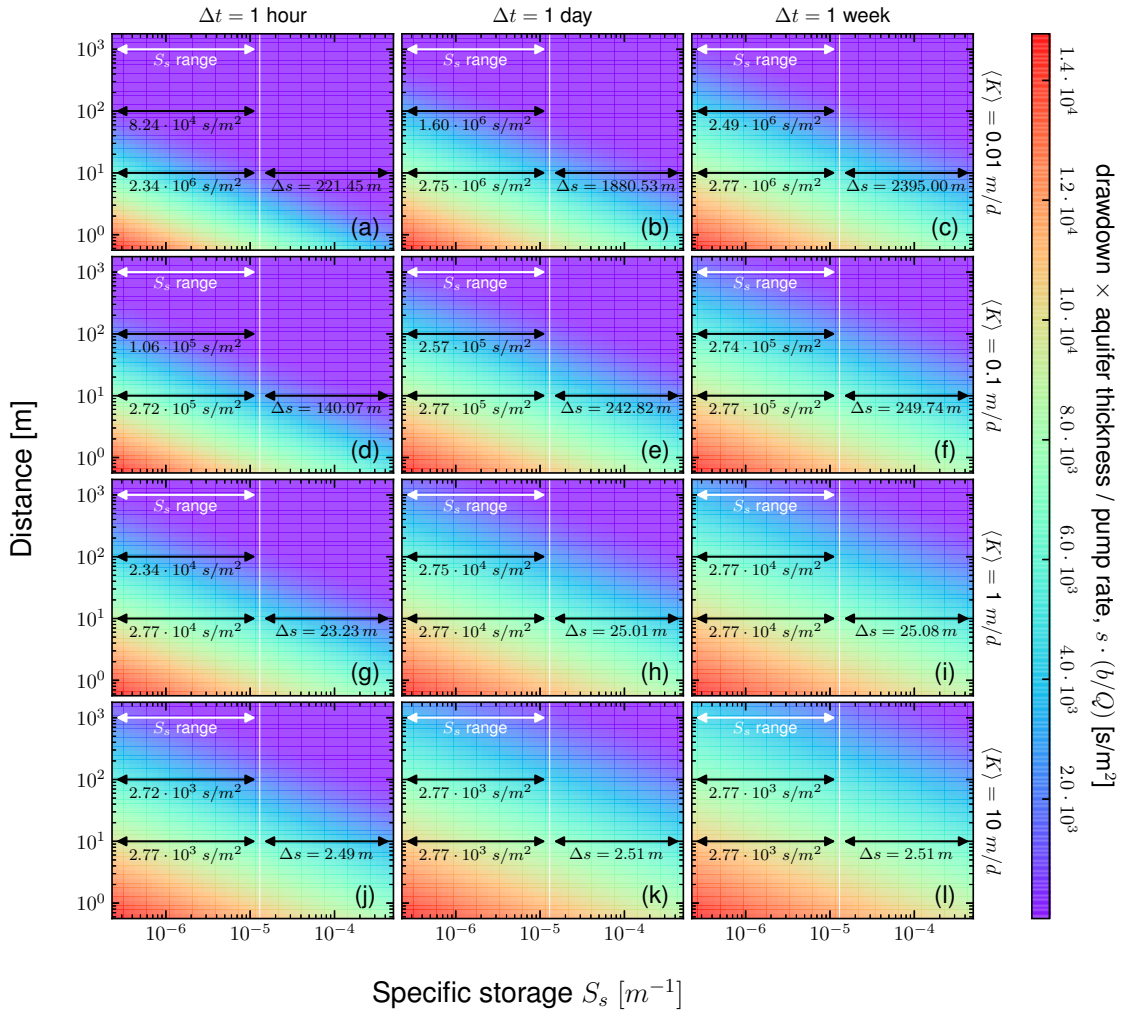
633 The uncertainty and lack of groundwater storage properties on a global scale [Richey
 634 *et al.*, 2015] has meant that groundwater models generally use crude estimates of this param-
 635 eter and also relegated it to a second-order importance. Even in aquifer testing interpretation,
 636 an order of magnitude estimate is often considered satisfactory [e.g. Kruseman and de Rid-
 637 der, 1990]. This is despite the fact that this also implies a high degree of uncertainty in the
 638 derived transmissivity value since these parameters appear together in commonly used *Well*
 639 *Functions* via the relationships for aquifer hydraulic diffusivity, $D = T/S = K/S_s$. Thus the
 640 accuracy of transmissivity and storage terms are inextricably linked.

641 Hsieh *et al.* [1988] consider the accuracy of specific storage values calculated theoretic-
 642 ally to only $\pm 50\%$. Such difficulty in obtaining representative aquifer storage values has
 643 meant that groundwater modeling has focused far more on transmissivity when trying to
 644 achieve satisfactory model calibration. The significance of variation in storage is almost al-
 645 ways overlooked, despite the fact that variation in storage can have just as great an impact on
 646 predicted groundwater elevations.

647 From the perspective of hydrogeology, which is mostly concerned with the continuous ex-
 648 traction of water from the subsurface, the poroelastic definitions *drained* and *undrained* (see
 649 Section 2.1) change over time. As water is removed from a bore, clearly there is a change
 650 in mass occurring and $d\zeta/dt = Q\rho_w$, where Q is the volume of water abstracted. How-
 651 ever, after a long time period of pumping from a confined aquifer, the system reaches steady-

652 state [Kruseman and De Ridder, 2000] and is at constant pore pressure ($dp/dt = 0$) as well
 653 as mass ($d\zeta/dt = 0$). By the poroelastic definitions given in Section 2.1, stress conditions
 654 become drained as soon as extraction starts but transition into undrained conditions when
 655 steady-state is reached. Drained and undrained elastic parameters can therefore be thought of
 656 as bounds for the poroelastic conditions encountered as a result of pumping.

657 A more complete consideration of poroelastic theory, as was undertaken in this paper, il-
 658 lustrates that the specific storage is limited to $2.3 \cdot 10^{-7} m^{-1} \lesssim S_s \lesssim 1.3 \cdot 10^{-5} m^{-1}$ with
 659 the lower limit derived from the poroelastic parameters of marble and the upper limit for ma-
 660 terials where the grain size is smaller than that of fine sands but where the adsorbed water
 661 fraction is small compared to the total water content.



662 **Figure 8.** Normalised drawdown [s/m^2] (i.e., Groundwater head drawdown (s) \times aquifer thickness (b) /
 663 pump rate (Q)) for a confined aquifer as calculated using the solution by Theis [1935]. To convert to draw-
 664 down in meters, multiply the values by Q/b . Notation on the left shows generic drawdown differences across
 665 the possible specific storage values of $2.3 \cdot 10^{-7} m^{-1} \lesssim S_s \lesssim 1.3 \cdot 10^{-5} m^{-1}$. Notation on the right illustrates
 666 our field example (Δs) across the possible specific storage values assuming our upper limit of S_s for discrete
 667 times, distances and hydraulic conductivities as well as a pumping rate of $Q = 50 L/s$ and an aquifer thickness
 668 of $b = 50 m$.

669 The uncertainty in S_s is substantial for estimating the drawdown caused by pumping. To
 670 illustrate the maximum possible drawdown difference due to our range in specific storage,
 671 Figure 8 shows the drawdown normalized by pumping rate and aquifer thickness for discrete
 672 pumping durations and realistic aquifer hydraulic conductivities ($\langle K \rangle = 0.01, 0.1, 1, 10$ m/d)
 673 estimated using the standard *Theis* [1935] solution. Interestingly, it appears that the differ-
 674 ence in normalized drawdown across the range of S_s is independent of the distance to the
 675 pumped well for high conductivities (Figure 8j-l) or long extraction periods (Figure 8f,i,l).

676 Where a groundwater model has performed a satisfactory mass balance using a very high
 677 storage coefficient, but we accept that such a value is not realistic based upon the known
 678 properties of the formation and the poroelastic theory described earlier, then we are forced
 679 to recognize that a large proportion of the water delivered can not come from storage changes
 680 within the formation. This must lead to a re-evaluation of the conceptual model of an aquifer
 681 and the inclusion of effective leakage into the modeled space, for example either from up-
 682 wards or downwards leakage through bounding aquitards or from lateral movement from
 683 channels associated with rivers or other recharge boundaries.

684 At our field sites, especially on the Liverpool Plains, uncertainty regarding specific stor-
 685 age persists in modeling groundwater resources where new coal mines are proposed, and
 686 there is a possibility of future coal-seam gas extraction. As very few, if any, measurements
 687 of specific storage in the low permeability units are available from pumping test studies, val-
 688 ues of specific storage in the range of $1 \cdot 10^{-6} m^{-1} \leq S_s \leq 5 \cdot 10^{-4} m^{-1}$ have been used
 689 to allow groundwater level calibration [*McNeilage, 2006; Price and Bellis, 2012*]. While
 690 the lower end is similar to values we have calculated from poroelastic analysis (an average of
 691 $\approx 2 \cdot 10^{-6} m^{-1}$), the upper value is at least an order of magnitude too high. The worst case dif-
 692 ference in drawdown resulting from lowering S_s to the upper bound determined here would
 693 be $\Delta s \approx 25$ m at a distance of 10 m from the extraction bore, assuming a hydraulic conduc-
 694 tivity of $\langle K \rangle = 1$ m/d, constant rate pumping $Q = 50$ L/s, aquifer thickness of $b = 50$ m
 695 (Figure 8g-i). Our analysis supports the observations of rapid downward leakage in response
 696 to pumping on the Liverpool Plains [*Timms and Acworth, 2004; Acworth and Timms, 2009*].

697 Our findings have global implications wherever groundwater models have been calibrated
 698 using values of specific storage that are unrealistically high ($\gg 1.3 \cdot 10^{-5} m^{-1}$). We should of
 699 course add the caveat that our poroelastic analysis is based upon the theory of linear poroe-
 700 lasticity and assumes perhaps an unwarranted degree of material homogeneity. However,
 701 use of the assumption that the *Biot-Willis* coefficient is unity will address this uncertainty.
 702 We anticipate that our results will help improve conceptual models that are used to quantify
 703 aquifer parameters for groundwater resource estimates and management.

704 4 Conclusions

705 We have derived new equations which relate the drained and undrained poroelastic param-
 706 eters governing specific storage in consolidated materials, incorporating the effects of both
 707 solid grain and bulk compressibility. We have shown how the necessary parameters can be
 708 derived from a combination of cross-hole seismic surveys and high frequency groundwater
 709 level measurements, reducing the large uncertainty that is normally inherent in storage esti-
 710 mates using a priori estimations of such parameters. Our new method for estimating specific
 711 storage relies on an estimation of formation density. However, this is relatively easy to con-
 712 strain in comparison with the assumptions inherent in other methods e.g. reliance of porosity
 713 values for tidal analysis [*Acworth et al., 2016a*] or the conceptual or numerical simplifica-
 714 tions applied during pumping test inversion [*Kruseman and De Ridder, 2000*].

715 We have presented field data and analysis to demonstrate the applicability of the new
 716 method in the context of two contrasting lithologies (sand, and smectite clay) and the re-
 717 sults show excellent agreement with those derived from an alternative method. Our results
 718 yield a new constraint of $S_s \lesssim 1.3 \cdot 10^{-5} m^{-1}$ for the physically plausible upper boundary of

719 specific storage for unconsolidated materials, applicable as long as the adsorbed water frac-
720 tion is small compared to the total water content. For clay-rich formations with substantial
721 adsorbed water, specific storage will be much lower than this value (as shown in Figure 6)
722 but in a range that is only as certain as the estimation of the free water content will allow.
723 This occurs because the adsorbed water significantly contributes to the compressibility of the
724 formation, but because it cannot flow under an imposed hydraulic gradient it thus does not
725 contribute to available groundwater storage .

726 It is common for literature values of specific storage of aquifers to be above the theoret-
727 ical maximum we present here. Where this is the case, a re-appraisal of the conceptual model
728 and data that have been used to derive such values is needed. This is critical to ensure more
729 robust management of groundwater resources from confined aquifers or to predict the pos-
730 sible subsidence due to continued groundwater abstraction, issues of increasing importance
731 worldwide.

732 **Acknowledgments**

733 The dataset for this work is freely accessible on *ResearchGate* (<https://dx.doi.org/10.13140/RG.2.2.31853.28646>). The Cattle Lane site was partly constructed using fund-
734 ing supplied by the *National Centre for Groundwater Research and Training (NCGRT)*, an
735 Australian Government initiative supported by the *Australian Research Council (ARC)* and
736 the *National Water Commission (NWC)*. The data used in this analysis was collected with
737 equipment provided by the Australian Federal Government financed *National Collaborative*
738 *Research Infrastructure Strategy (NCRIS)*. The groundwater data is available through the
739 *NCRIS Groundwater Database*: <http://groundwater.anu.edu.au>. We acknowledge
740 the excellent *Matplotlib v2.1.2* library [Hunter, 2007] which was used to generate most of
741 the figures. GCR was partly supported by the *NCGRT*. LJSH was partly supported by the
742 *Swiss National Science Foundation (SNF/FNS)*, project 166233. Funding is gratefully ac-
743 knowledged by MOC for an Independent Research Fellowship from the UK Natural Envi-
744 ronment Research Council (NE/P017819/1). We thank Dayna McGeeney for conducting the
745 core moisture and density analyses, and Hamish Studholme for supervising the drilling and
746 coring work.
747

Appendix

Variable	Definition and SI Units
<i>ads</i>	(subscript) Adsorbed water
<i>free</i>	(subscript) Free water
<i>s</i>	(subscript) Solid matrix
<i>w</i>	(subscript) Water
<i>v</i>	(subscript) Vertical
<i>h</i>	(subscript) Horizontal
<i>u</i>	(superscript) Undrained
< <i>none</i> >	(superscript) Drained
<i>B</i>	Skempton coefficient [-]
<i>BE</i>	Barometric Efficiency [-]
$E^{(u)}$	Young's Modulus [Pa]
<i>g</i>	Acceleration due to gravity [m/s ²]
<i>G</i>	Shear (or rigidity) modulus [Pa]
$K^{(u)}$	Modulus of elasticity [Pa]
$K^{(u)}$	Uniaxial (horizontal or vertical) or confined modulus of elasticity [Pa]
<i>l</i>	Length [m]
<i>LE</i>	Uniaxial loading efficiency [-]
M_2^{ET}	M_2 Earth tide amplitude ^a [m/s ²]
M_2^{GW}	M_2 Groundwater amplitude ^a [m H ₂ O or Pa]
<i>p</i>	Pressure [Pa]
<i>h</i>	Groundwater head [m]
<i>S_s</i>	Specific storage [m ⁻¹]
<i>S_y</i>	Specific yield [-]
S_2^{AT}	S_2 Atmospheric tide amplitude ^a [m H ₂ O or Pa]
S_2^{ET}	S_2 Earth tide amplitude ^a [m/s ²]
S_2^{GW}	S_2 Groundwater amplitude ^a [m H ₂ O or Pa]
<i>V</i>	Volume [m ³]
<i>V_p</i>	Seismic P-wave velocity [m/s]
<i>V_s</i>	Seismic S-wave velocity [m/s]
<i>α</i>	Biot-Willis coefficient [-]
$\beta^{(u)}$	Compressibility [Pa ⁻¹]
$\Delta\phi$	Phase shift [rad]
<i>ε</i>	Strain [Pa ⁻¹]
$\lambda^{(u)}$	Lamé's modulus [-]
$\mu^{(u)}$	Poisson's Ratio [-]
<i>ρ</i>	Bulk density [kg/m ³]
<i>σ</i>	Stress [Pa]
<i>θ</i>	Total porosity (= water content in saturated zone) [-]
<i>z</i>	Depth [m]
<i>s</i>	Change in head with pumping (drawdown) [m]
<i>b</i>	Aquifer thickness [m]
<i>(K)</i>	Hydraulic conductivity [m/s]
<i>Q</i>	Pumping rate [m ³ /s]

Table 2. Definitions of variables used. ^a See Acworth *et al.* [2016a].

References

- 751 Acworth, R. (2007), Measurement of vertical environmental-head profiles in unconfined sand
752 aquifers using a multi-channel manometer board, *Hydrogeology Journal*, 15(7), 1279–
753 1289, doi:10.1007/s10040-007-0178-9, first Online: 13 April 2007.
- 754 Acworth, R., and J. Jankowski (1993), Hydrogeochemical zonation of groundwater in the
755 botany sands aquifer, sydney, *AGSO Journal of Australian Geology*, 14(2), 193–200.
- 756 Acworth, R., and L. Jorstad (2006), Integration of multi-channel piezometry and electrical
757 tomography to better define chemical heterogeneity in a landfill leachate plume within
758 a sand aquifer, *Journal of Contaminant Hydrology*, 83(3-4), 200–220, doi:10.1016/j.
759 jconhyd.2005.11.007.
- 760 Acworth, R., and W. Timms (2009), Evidence for connected water processes through
761 smectite-dominated clays at breeza, new south wales, *Australian Journal of Earth Sci-*
762 *ences*, 56(1), 81–96, doi:10.1080/08120090802541952.

- 763 Acworth, R., W. Timms, B. Kelly, D. McGeeney, T. Ralph, Z. Larkin, and G. Rau (2015),
 764 Late Cenozoic paleovalley fill sequence from the southern Liverpool Plains, New South
 765 Wales - implications for groundwater resource evaluation, *Australian Journal of Earth*
 766 *Sciences*, 62, 657–680, doi:10.1080/08120099.2015.1086815.
- 767 Acworth, R., L. Halloran, G. Rau, M. Cuthbert, and T. Bernadi (2016a), An objective
 768 method to quantify groundwater compressible storage using earth and atmospheric tides,
 769 *Geophysical Research Letters*, 43(22), 11,671–11,678, doi:10.1002/2016gl071328, sub-
 770 mitted 27 September 2016.
- 771 Acworth, R., G. Rau, M. Cuthbert, E. Jensen, and K. Leggett (2016b), Long-term spatio-
 772 temporal precipitation variability in arid-zone australia and implications for groundwater
 773 recharge, *Hydrogeology Journal*, 24(4), 905–921.
- 774 Acworth, R. I., G. C. Rau, L. J. Halloran, and W. A. Timms (2017), Vertical groundwa-
 775 ter storage properties and changes in confinement determined using hydraulic head re-
 776 sponse to atmospheric tides, *Water Resources Research*, 53(4), 2983–2997, doi:10.1002/
 777 2016WR020311.
- 778 Alley, W. M., R. W. Healy, J. W. LaBaugh, and T. E. Reilly (2002), Flow and storage in
 779 groundwater systems, *Science*, 296, doi:10.1126/science.1067123.
- 780 Bathija, A. P. (2000), Elastic properties of clays, Ph.D. thesis, Colorado School of Mines.
- 781 Biot, M. (1941), General theory of three-dimensional consolidation, *Journal of Applied Geo-*
 782 *physics*, 12, 155–164.
- 783 Bowler, J. (1990), The last 500,000 years, in *The Murray*, edited by N. Mackay and
 784 D. Eastburn, pp. 95–104, The Murray-Darling Basin Commission, The Murray-Darling
 785 Basin Commission, Canberra, Australia.
- 786 Bredehoeft, J. D., and R. L. Cooley (1983), Comment on “a note on the meaning of storage
 787 coefficient by T. N. Narasimhan and B. Y. Kanehiro”, *Water Resources Research*, 19(6),
 788 1632–1634, doi:10.1029/WR019i006p01632.
- 789 Clayton, C. (2011), Stiffness at small strain: research and practice, *Geotechnique*, 61(1), 5–
 790 37, doi:10.1680/geot.2011.61.1.5.
- 791 Cooper, H. (1966), The equation of groundwater flow in fixed and deforming coordinates,
 792 *Journal of Geophysical*, 71(20), 4785–4790, doi:10.1029/JZ071i020p04785.
- 793 Crice, D. (2011), Near-surface, downhole shear-wave surveys: A primer, *The Leading Edge:*
 794 *GEOPHYSICS*, pp. 164–171.
- 795 David, K., W. Timms, S. Barbour, and R. Mitra (2017), Tracking changes in the specific stor-
 796 age of overburden rock during longwall coal mining, *Journal of Hydrology*, 553, 304 –
 797 320, doi:https://doi.org/10.1016/j.jhydrol.2017.07.057.
- 798 Davis, A. (1989), Determination of dynamic elastic parameters from crosshole testing, *Scien-*
 799 *tific Drilling*, 1(1), 54–62.
- 800 Davis, A., and D. Taylor-Smith (1980), Dynamic elastic moduli logging of foundation ma-
 801 terials, in *Offshore Site Investigation*, edited by D. Ardu, Graham and Trotman, pages
 802 21–132.
- 803 Domenico, P. (1983), Determination of bulk rock properties from ground-water level fluctua-
 804 tions, *Environmental and Engineering Geoscience*, (3), 283–287, doi:10.2113/gseegeosci.
 805 xx.3.283.
- 806 Domenico, P., and F. Schwartz (1997), *Physical and Chemical Hydrogeology*, 2nd ed., John
 807 Wiley and Sons.
- 808 Fetter, C. (2001), *Applied Hydrogeology*, fourth ed., Prentice Hall, Upper Saddle River, New
 809 Jersey 07458, USA.
- 810 Galperin, A., V. Zaytsev, A. Yu, and Y. Norvatov (1993), *Hydrogeology and Engineering*
 811 *Geology*, A.A. Balkema, Rotterdam, translated from Russian and edited by R.B. Zeidler of
 812 H*T*S*, Gdańsk.
- 813 Gleeson, T., W. M. Alley, D. M. Allen, M. A. Sophocleous, Y. Zhou, M. Taniguchi, and
 814 J. VanderSteen (2012), Towards sustainable groundwater use: setting long-term goals,
 815 backcasting, and managing adaptively, *Groundwater*, 50(1), 19–26, doi:10.1111/j.
 816 1745-6584.2011.00825.x.

- 817 Green, D., and H. Wang (1990), Storage as a poroelastic coefficient, *Water Resources Re-*
 818 *search*, 26(7), 1631–1637, doi:10.1029/WR026i007p01631.
- 819 Hantush, M. S. (1960), Modification of the theory of leaky aquifers, *Journal of Geophysical*
 820 *Research*, 65(11), 3713–3725, doi:10.1029/JZ065i011p03713.
- 821 Hantush, M. S. (1967a), Flow of groundwater in relatively thick leaky aquifers, *Water Re-*
 822 *sources Research*, 3(2), 583–590, doi:10.1029/WR003i002p00583.
- 823 Hantush, M. S. (1967b), Flow to wells in aquifers separated by a semipervious layer, *Journal*
 824 *of Geophysical Research*, 72(6), 1709–1720, doi:10.1029/JZ072i006p01709.
- 825 Hsieh, P. A., J. D. Bredehoeft, and S. A. Rojstaczer (1988), Response of well aquifer systems
 826 to earth tides: Problem revisited, *Water Resources Research*, 24(3), 468–472, doi:10.1029/
 827 WR024i003p00468.
- 828 Hunter, J. D. (2007), Matplotlib: A 2d graphics environment, *Computing In Science & Engi-*
 829 *neering*, 9(3), 90–95, doi:10.1109/MCSE.2007.55.
- 830 Jacob, C. (1940), On the flow of water in an elastic artesian aquifer, *Transactions American*
 831 *Geophysics Union*, 21(2), 574–586, doi:10.1029/TR021i002p00574.
- 832 Jury, W., W. Gardner, and W. Gardner (1991), *Soil Physics*, fifth ed., John Wiley & Sons, inc.
- 833 Kruseman, G., and N. de Ridder (1990), Analysis and evaluation of pumping test data, *Pub-*
 834 *lication 47*, International Institute for Land Reclamation and Improvement, P.O. Box 45,
 835 6700 AA Wageningen, The Netherlands, 1994, Second Edition (Completely Revised).
- 836 Kruseman, G., and N. De Ridder (2000), *Analysis and Evaluation of Pumping Test Data*,
 837 vol. 47, 2nd edition ed., ILRI.
- 838 Martin, R. (1960), Adsorbed water on clay: A review, *Clays and Clay Minerals*, 9(1), 28–70,
 839 doi:10.1346/CCMN.1960.0090104.
- 840 Mathews, M., V. Hope, and C. Clayton (1994), The geotechnical value of ground stiffness
 841 determined using seismic methods, in *Modern Geophysics in Engineering Geology, EGAC*
 842 *94 - Proceedings of 30th Annual Conference of the Engineering Group of the Geological*
 843 *Society, University of Liege, Belgium, 1994*, pp. 7–12, The Geological Society of London.
- 844 McNeilage, C. (2006), Upper namoi groundwater flow model: Model development and cali-
 845 bration, *Tech. rep.*, Australian Government, New South Wales Department of Natural Re-
 846 sources.
- 847 Meinzer, O. E. (1928), Compressibility and elasticity of artesian aquifers, *Economic Geol-*
 848 *ogy*, 23(3), 263–291, doi:10.2113/gsecongeo.23.3.263.
- 849 Narasimhan, T. (1979), The significance of the storage parameter in saturated-unsaturated
 850 groundwater flow, *Water Resources Research*, 15(3), 569–576, doi:10.1029/
 851 WR015i003p00569.
- 852 Narasimhan, T. (1983), Reply, *Water Resources Research*, 19(6), 1630–1640, doi:10.1029/
 853 WR019i006p01636.
- 854 Narasimhan, T., and B. Kanehiro (1980), A note on the meaning of storage coefficient, *Water*
 855 *Resources Research*, 16(2), 423–429, doi:10.1029/WR016i002p00423.
- 856 Palciauskas, V., and P. Domenico (1989), Fluid pressures in deforming porous rocks, *Water*
 857 *Resources Research*, 25(2), 203–213, doi:10.1029/WR025i002p00203.
- 858 Petit, J., J. Jouzel, D. Raynaud, J. M. Barkov, N.I. Barnola, I. Basile, M. Bender, J. Chap-
 859 pellaz, M. Davis, G. Delaygue, M. Delmotte, V. M. Kotlyakpv, M. Legrand, V. Lipenkov,
 860 C. Lorius, L. Pepin, C. Ritz, E. Saltzman, and M. Stievenard (1999), Climate and atmo-
 861 spheric history of the past 420,000 years from the Vostok ice core, Antarctica, *Nature*,
 862 399(3), 429–436.
- 863 Prasad, M., M. Kopycinska, U. Rabe, and W. Arnold (2001), Measurement of young's mod-
 864 ulus of clay minerals using atomic force acoustic microscopy, *Geophysical Research Let-*
 865 *ters*, 29(8), 13–1–13–4, doi:10.1029/2001GL014054.
- 866 Price, G., and L. Bellis (2012), Namoi catchment water study - independent expert - final
 867 study report, *Tech. Rep. 50371/P4-R2 FINAL*, Schlumberger Water Services (Australia)
 868 Pty Ltd, department of Trade and Investment, Regional Infrastructure and Services, New
 869 South Wales, (DTIRIS NSW) Locked Bag 21 Orange NSW 2800 Australia.

- 870 Richardson, N., K. Williams, K. Briggs, and E. Thorsos (2002), Dynamic measurement of
871 sediment grain compressibility at atmospheric pressure: acoustic applications, *IEEE Jour-*
872 *nal of Oceanic Engineering*, 27(3), 593–601, doi:10.1109/JOE.2002.1040941.
- 873 Richey, A. S., B. F. Thomas, M.-H. Lo, J. S. Famiglietti, S. Swenson, and M. Rodell (2015),
874 Uncertainty in global groundwater storage estimates in a total groundwater stress frame-
875 work, *Water Resources Research*, doi:10.1002/2015WR017351.
- 876 Theis, C. (1935), The relationship between the lowering of the piezometric surface and the
877 rate and duration of discharge of a well using groundwater storage, *Transactions American*
878 *Geophysical Union*, 2, 519–524.
- 879 Timms, W., and R. Acworth (2004), Induced leakage through aquitard fractures and windows
880 - impacts on groundwater quality at irrigation sites, in *The 9th Murray-Darling Basin*
881 *Groundwater Workshop 2004*.
- 882 Van Der Kamp, G., and J. Gale (1983), Theory of earth tide and barometric effects in porous
883 formations with compressible grains, *Water Resources Research*, 19(2), 538–544, doi:
884 10.1029/WR019i002p00538.
- 885 Verruijt, A. (2016), *Theory and Problems of Poroelasticity*, self published.
- 886 Wada, Y., L. P. H. v. Beek, N. Wanders, and M. F. Bierkens (2013), Human water consump-
887 tion intensifies hydrological drought worldwide, *Environmental Research Letters*, 8.
- 888 Wang, H. F. (2000), *Theory of Linear Poroelasticity with Applications to Geomechanics and*
889 *Hydrogeology (Princeton Series in Geophysics)*, Princetown University Press.
- 890 Webb, S., and K. Watson (1979), Hydraulic behaviour of an unconfined aquifer, *Technical*
891 *Paper 38*, Australian Water Resources Council, Australian Government Publishing Ser-
892 vice, Canberra.